Theoretical analysis of d–d transitions for the reduced Cr/silica system

Øystein Espelid and Knut J. Børve

Department of Chemistry, University of Bergen, Allégaten 41, N-5007 Bergen, Norway
E-mail: oystein.espelid@kj.uib.no; knut.borve@kj.uib.no

Received 10 April 2001; accepted 10 May 2001

Cluster models are constructed for mono- and dinuclear Cr(II) sites and mononuclear Cr(III) sites on the Cr/SiO_2 Phillips catalyst and used to compute d–d transition energies and intensities. Mononuclear pseudo-tetrahedral Cr(II) gives rise to two bands of electric-dipole-allowed d–d transitions, at 8,400 and 12,300 cm^{-1}. This doublet is lowered in energy and intensity as the bond angle about chromium, ∠OCrO, opens up. The dinuclear site gives rise to bands at 5,200 and 10,300 cm^{-1}, consistent with calculations for a mononuclear cluster of comparable value for ∠OCrO. A tri-coordinated Cr(III) cluster shows bands of comparable oscillator strengths at energies of 11,000, 16,000, 18,000–20,000 and 33,000 cm^{-1}. The predicted bands correspond well with d–d bands in experimental diffuse reflectance spectra.

KEY WORDS: electronic transitions; d–d spectra; Phillips catalysis; CASPT2; cluster models

1. Introduction

Diffuse reflectance spectroscopy (DRS) has recently been launched as a suitable technique for studying heterogeneous catalysis, as both d–d and charge-transfer transitions of supported transition metal ions can be probed [1]. In particular, DRS has been used to address the long-standing question of the active oxidation state of chromium in Phillips catalysts. These Cr/SiO_2(s)-based catalysts are responsible for more than one-third of the world production of polyethylene-based polymers [2], yet they remain somewhat of an enigma in terms of microscopic composition and structure.

In the calcined catalyst, chromium is in its hexavalent state, either predominantly as monochromate species, *e.g.*, on pyrogenic silica supports at low chromium loadings, or both dichromate and monochromate, as found on industrial sol–gel silica [3]. The catalyst is reduced before attaining full activity, either during the early stages of contact with ethylene or, in a separate pretreatment step, by exposing the catalyst to carbon monoxide at elevated temperatures [4]. It is widely believed that after reduction, the dominating chromium species is divalent [3], with the remaining chromium present either as unreactive chromia particles [5] or as isolated Cr(III) species [6]. The identification of Cr(II) as the dominating oxidation state is corroborated by IR spectra of chromium-carbonyl species, which have been interpreted in terms of mononuclear (pseudo-) tetrahedral chromium(II) species on pyrogenic silica [7] and both mono- and dinuclear species on sol–gel silica [8]. Re-oxidation of the catalyst reestablishes the initial monochromate-to-dichromate ratio, suggesting a connection between the nuclearity of surface species of the calcined and reduced catalyst [6].

Diffuse reflectance spectroscopy of the reduced catalyst reveals two broad bands in the d–d region. Transitions in the 7,000–10,000 and 10,000–13,000 cm^{-1} regions have been assigned to pseudo-tetrahedral and pseudo-octahedral Cr(II), respectively [9]. Hence, more than identifying oxidation states, DRS characterization studies have been used to differentiate between Cr(II) in different local surroundings. While this is an important step in the direction of identifying the active site(s) in the Phillips catalyst, one should bear in mind that assignation of the broad d–d bands is hampered by the lack of knowledge of the number and positions of the observable electronic transitions. For instance, all known coordination states of Cr(II) yield d–d bands in the region 5,000–14,000 cm^{-1} [5,10]. On this background, there is a need for theoretical calculations on models of supported transition-metal ions [2].

The aim of the present work is to aid future analyses of the d–d region in DRS spectra of reduced Phillips-type catalysts as well as model systems thereof. We have constructed cluster models of coordinatively unsaturated mononuclear and dinuclear Cr(II) sites, with mononuclear Cr(II) bound at sites that differ with respect to the sterical constraints. Furthermore, a model of mononuclear Cr(III) covalently bound to three surface oxygen atoms, has been prepared. State-of-the-art quantum chemical methods are then applied to calculate electronic d–d transition energies and electric-dipole oscillator strengths. The resulting spectroscopic information is used to discuss assignment in the d–d region (7,000–21,000 cm^{-1}) of DRS spectra of Phillips-type model systems.

1011-372X/01/0800-0049$19.50/0

2. Computational models

2.1. Basis sets and methods

The cluster models were studied in their ground-state geometries, optimized using the hybrid gradient-corrected density functional method B3LYP [11–13], as implemented in the Gaussian-98 program [14].

Molecular orbitals were formed in gaussian-type atom-centered bases of triple-ζ quality (or better) as extended by diffuse and polarization functions. For H, O, F and Cr, the basis sets denoted by *TZD1P* in [15] were used, albeit with a set of contracted f functions added to Cr [16] and with d functions on O and F redefined by $\alpha_d = 1.292$ and 1.750, respectively. Silicon was described by a (12s9p)/[6s5p] basis [17], augmented by a set of even-tempered, diffuse s and p functions and a single set of polarization functions ($\alpha_d = 0.450$).

Transition energies were computed from second-order, multi-reference many-body perturbation theory as implemented in the CASPT2 module [18] of Molcas-4 [19]. The reference states were determined at the restricted CASSCF [20] level of theory, with an active space consisting of the singly-occupied orbitals as well as any virtual Cr 3d orbitals. When optimizing orbitals for excited states, a low weight (1%) was assigned to each interacting state of lower energy than that of the state sought, to avoid root flipping. All valence electrons were correlated in the subsequent CASPT2 step in order to account for dynamical correlation energy. Electric-dipole transition moments were obtained from CASSCF wave functions in the length representation [21], using the RASSI approach [22].

2.2. Cluster models

The dominating mononuclear chromium species of the reduced catalyst is divalent and bound by two oxygen ester linkages to the surface. Based on the ∠OCrO bond angle, these divalent species may be classified further into pseudo-tetrahedral and pseudo-octahedral Cr(II) surface species. An unstrained ∠OCrO bond angle of a reduced chromium surface species is expected to lie in the vicinity of 150°, *i.e.*, close to the ∠OCrO bond angle of $Cr(OH)_2(g)$ [15]. Thus, the silica surface must present some strain on the chromium sites to support a distribution of pseudo-tetrahedral to pseudo-octahedral divalent chromium surface species.

The mononuclear Cr(II) surface species are represented by three cluster models (see figure 1); a pseudo-tetrahedral site (**T**) (left); a pseudo-octahedral site (**O**) (right); and, a site with an intermediate ∠OCrO bond angle (**I**) (center). The **T** and **I** cluster models are similar to those used in previous work on the reactivity of these sites [23], except that fluorine replaces hydrogen as terminating agent. Guided by previous studies of silanol groups at the silica surface [24], the octahedral cluster was terminated by trifluorosilanol moieties, to make $Cr(OSiF_3)_2$. The basic electronic properties of this

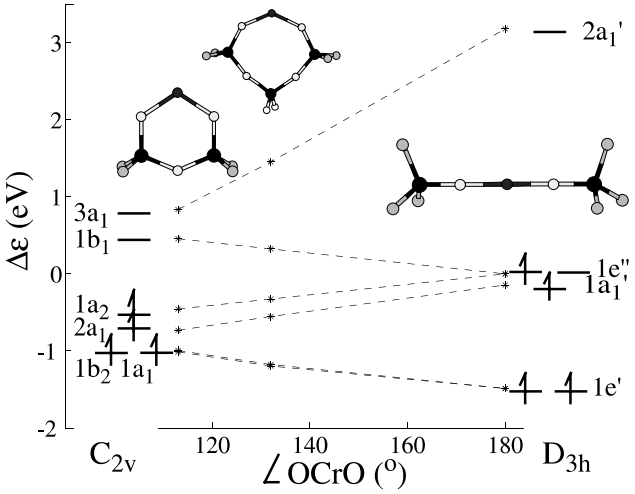

Figure 1. Walsh diagram of the molecular orbitals with mainly chromium 3d and 4s character for divalent mononuclear chromium cluster models with the OCrO bond angle in the tetrahedral-to-octahedral range. Orbital energies are shown relative to the mean energy of the highest occupied and the lowest unoccupied orbitals in the ground state, and with all virtual levels uniformly shifted to reflect the energy of the lowest d–d transition. The elements are coded on a gray scale according to increasing atom number H (white) < O < F < Si < Cr (dark gray).

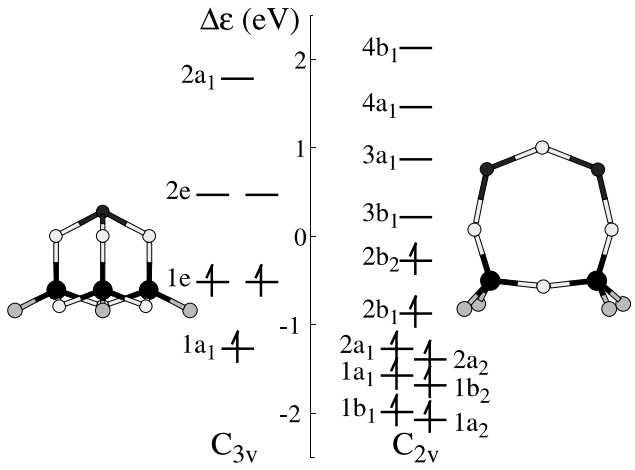

Figure 2. Orbital energy diagrams for a mononuclear, trivalent chromium cluster (**fac-Cr(III)**, left), and a dinuclear, divalent chromium cluster (**D**, right). Preparation of relative orbital energies and explanation to the gray-scale coding is given in figure 1.

model were validated by comparison to a much larger cluster in which the anchoring site was represented by two singly-deprotonated hydroxosilasesquioxane clusters. While geometry parameters and atomic charges are virtually identical for the two clusters, there is a close-to uniform shift of 0.75 eV in 3d orbital energies. However, the constancy of the shift makes d–d transitions energies agree well between the two models.

Our model of a dinuclear chromium(II) surface species was constructed by attaching a –OCrOCrO– unit to an anchoring site similar to that used for the mononuclear **T** cluster. The resulting cluster model is shown to the right in figure 2 and will be denoted by **D**.

Table 1
Selected geometry parameters of the cluster models, mononuclear Cr(II): tetrahedral (**T**), intermediate (**I**) and octahedral (**O**); dinuclear Cr(II) (**D**); and mononuclear **fac-Cr(III)**.[a]

	r_{CrO}	r_{SiO}	∠OCrO	∠SiOCr
Cr(II) **T**	1.839	1.619	107.9	127.4
Cr(II) **I**	1.818	1.631	132.3	140.8
Cr(II) **O**	1.845	1.605	180.0	180.0
Cr(II) **D**[b]	1.839	1.603	123.8	150.6
fac-Cr(III)	1.811	1.651	104.0	114.0

[a] Units: bond length (r) in (Å), angle (∠) in degrees.
[b] Geometry parameters unique to **D**: $r_{CrO_{bridge}}$ 1.803 Å, ∠CrOCr 137.5°.

The mononuclear chromium(III) site was represented by a single cluster model, prepared by anchoring chromium to a ring of three silanol moieties bound to one another through oxygen bridges. The resulting cluster model possesses C_{3v} symmetry and is shown to the left in figure 2.

Geometry parameters describing the coordination sphere of chromium, are included in table 1 for all the clusters used. In structures of C_{2v} symmetry, σ_v denotes the symmetry plane that contains a CrO_2 moiety.

3. Results

3.1. Mononuclear Cr(II) sites

A Walsh diagram for the molecular orbitals with considerable chromium 3d and 4s character is shown in figure 1, for mononuclear Cr(II) clusters displaying a ∠OCrO bond angle in the tetrahedral-to-octahedral range.

The two lowest-lying orbital energy levels shown for the pseudo-octahedral conformation, $1e'$ and $1a_1'$, correspond to orbitals that are non-bonding and mainly of Cr $3d_\delta$ and "$3d_\sigma + 4s$" character, respectively. The next two orbitals, $1e''$ and $2a_1'$, have π^* and σ^* anti-bonding character toward the ester oxygens, with large Cr $3d_\pi$ and "$3d_\sigma - 4s$" components, respectively. Since the $1e''$ shell accommodates only a single electron in the ground state, the term symbol becomes $^5E''$.

Upon bending the ∠OCrO bond angle away from linear arrangement, the most pronounced effects are seen for the anti-bonding molecular orbitals. The $1e''$ level splits into $1a_2$ and $1b_1$, and the $1a_2$ orbital receives the single electron because of less π^* character. The $1b_1$ orbital is thus unoccupied and becomes increasingly anti-bonding toward the ester oxygens, displaying both π^* and σ^* character. The largest change in stability is seen for the unoccupied $2a_1'$ ($3a_1$) orbital, due to decreasing σ^* character. Only minor changes are observed for $1e'$ and $1a_1'$ as they transform into orbitals of a_1 and b_2, and a_1 symmetry, respectively, making $^5B_1$ the ground state.

Vertical d–d transition energies of the mononuclear Cr(II) clusters are presented in table 2. Starting with the pseudo-tetrahedral cluster model (**T**), the four lowest d–d transitions correspond to excitation of an electron from one of the four singly-occupied molecular orbitals into the lowest unoccupied molecular orbital, $1b_1$. Only two of these

Table 2
Computed d–d transition energies (T) and oscillator strengths (f) for mononuclear Cr(II) clusters.

Transition	T (cm^{-1})	$f \times 10^5$
Pseudo-tetrahedral (**T**)		
$1\,^5A_1 \leftarrow 1\,^5B_1$	7,700	0
$1\,^5A_2 \leftarrow 1\,^5B_1$	8,400	17
$1\,^5B_2 \leftarrow 1\,^5B_1$	12,000	0[a]
$2\,^5A_1 \leftarrow 1\,^5B_1$	12,300	17
Intermediate (**I**)		
$1\,^5A_1 \leftarrow 1\,^5B_1$	4,700	2
$1\,^5A_2 \leftarrow 1\,^5B_1$	4,900	5
$1\,^5B_2 \leftarrow 1\,^5B_1$	10,700	0[a]
$2\,^5A_1 \leftarrow 1\,^5B_1$	10,800	8
Pseudo-octahedral (**O**)		
$1\,^5A_1' \leftarrow 1\,^5E''$	−900	0[a]
$1\,^5E' \leftarrow 1\,^5E''$	7,200	0

[a] Symmetry-forbidden in C_{2v} (**T**, **I**) or D_{3h} (**O**).

transitions receive an appreciable electric-dipole oscillator strength, namely $1b_1 \leftarrow 1a_2$ and $1b_1 \leftarrow 1a_1$, at transition energies of 8,400 and 12,300 cm^{-1}, respectively. The other two transitions may gain some intensity through coupling to vibrational degrees of freedom. However, since the transition energies coincide well with those of the dipole-allowed transitions, additional structure in the spectrum is not expected.

A second set of excitations have their origin in the promotion of an unpaired electron into $3a_1$, which has notable components at the ester oxygens. This gives the excitations a mixed d–d and metal-to-ligand character, resulting in high transition energies and large oscillator strengths. The lowest of these excitations, $3a_1 \leftarrow 1a_2$, is electric-dipole forbidden and has an energy of 27,000 cm^{-1}. The other three are found with energies of 29,000–30,000 cm^{-1} and with oscillator strengths between 0.002 and 0.03. However, since there are other transitions that may contribute to spectral density in the charge-transfer region, our results do not open for interpretation of this part of the spectrum.

As is apparent in the Walsh diagram, figure 1, the energy gap between the $1b_1$ and $1a_2$ orbitals decreases steadily with increasing ∠OCrO bond angle. Hence, the main change in the d–d spectrum upon going from **T** to the **I** cluster (∠OCrO = 132°), is a shift to lower transition energies. The pattern of two distinct bands prevails, but now shifted to 4,900 and 10,800 cm^{-1}. The associated oscillator strengths are also notably lower, *cf.* table 2.

The trend of converging orbital energies continues to full degeneracy at the pseudo-octahedral site. Moreover, the close proximity of $1a'$ and $1e''$ makes it difficult to ascertain the ground state of the **O** cluster. While density-functional theory predicts a ground-state electronic configuration of $(1e')^2(1a_1')^1(1e'')^1$, Hartree–Fock has a strong bias toward $(1e')^2(1e'')^2$, to the extent that even at the CASPT2 level of theory, the latter is lower, by 900 cm^{-1}. Going to even more accurate theories, the energy difference between these two states is reduced to 200 cm^{-1}, without really resolving the

Table 3
Computed d–d transition energies (T) and electric-dipole oscillator strengths (f) for the dinuclear chromium(II) cluster **D**.

Transition	T (cm^{-1})	$f \times 10^5$	Orbital transitions
$1\,^9A_2 \leftarrow 1\,^9A_1$	3,600	0[a]	$2a_2 \rightarrow 3a_1$; $2b_2 \rightarrow 3b_1$
$2\,^9A_1 \leftarrow 1\,^9A_1$	4,200	3	$2a_1 \rightarrow 3a_1$; $2b_1 \rightarrow 3b_1$
$1\,^9B_1 \leftarrow 1\,^9A_1$	4,700	2	$2a_1 \rightarrow 3b_1$; $2b_1 \rightarrow 3a_1$
$1\,^9B_2 \leftarrow 1\,^9A_1$	5,200	16	$2b_2 \rightarrow 3a_1$; $2a_2 \rightarrow 3b_1$
$2\,^9B_2 \leftarrow 1\,^9A_1$	10,000	0	$(2b_2, 2b_1) \rightarrow (3a_1, 3b_1)$
			$(2a_1, 2a_2) \rightarrow (3a_1, 3b_1)$
$2\,^9A_2 \leftarrow 1\,^9A_1$	10,100	0[a]	$1a_2 \rightarrow 3a_1$; $1b_2 \rightarrow 3b_1$
$2\,^9B_1 \leftarrow 1\,^9A_1$	10,300	14	$1a_1 \rightarrow 3b_1$; $1b_1 \rightarrow 3a_1$
$3\,^9A_1 \leftarrow 1\,^9A_1$	10,400	9	$1a_1 \rightarrow 3a_1$; $1b_1 \rightarrow 3b_1$
$3\,^9B_2 \leftarrow 1\,^9A_1$	10,700[b]	0	$1b_2 \rightarrow 3a_1$; $1a_2 \rightarrow 3b_1$
$3\,^9A_2 \leftarrow 1\,^9A_1$	10,800	0[a]	$(2a_1, 2b_2) \rightarrow (3a_1, 3b_1)$
			$(2a_2, 2b_1) \rightarrow (3a_1, 3b_1)$
$4\,^9A_1 \leftarrow 1\,^9A_1$	11,500	0	$(2a_1, 2b_1) \rightarrow (3a_1, 3b_1)$

[a] Symmetry forbidden in C_{2v}.
[b] Orbitals optimized in a state-average CASSCF calculation, with weight factors of 15, 15 and 70% on the first three roots of $^9B_2$ symmetry, respectively.

issue of the ground state. Here it suffices to conclude that the linear, pseudo-octahedral site gives rise to a single d–d band, at a transition energy in the range 7,000–8,000 cm^{-1}. Since the transition is electric-dipole forbidden and, moreover, at least partly overlapping with a relatively strong band from the tetrahedral sites, it may be difficult to use d–d transitions to identify pseudo-octahedral sites.

3.2. Dinuclear Cr(II) sites

The molecular orbitals of the dinuclear, divalent chromium cluster may be understood as symmetrized analogous of orbitals already described for the mononuclear case. This implies that each electronic transition is typically described by two one-electron excitations, making a multi-reference description mandatory. Electronic d–d transitions derive their intensities from excitation of unpaired d electrons into the virtual $3b_1$ and $3a_1$ orbitals, *cf.* the *right* side of figure 2. When proper account of configuration interaction is made, the spectrum emerging in table 3 is one quite similar to that of the intermediate mononuclear cluster, **I**. There are two electric-dipole-allowed bands, one at 10,300 cm^{-1}, consisting of two transitions, and a low-energy band at 5,200 cm^{-1}. The resemblance to the spectrum computed for **I** suggests that at least in the d–d region, the dinuclear site is acting as two mononuclear sites of matching ∠OCrO bond angle.

In addition to the dominating electric-dipole bands, the dinuclear cluster shows several dipole-forbidden transitions below 5,000 cm^{-1}. In agreement with this, the lowest doubly-excited state is found as low in energy as 10,000 cm^{-1}, albeit with negligible oscillator strength in the dipole approximation. Doubly-excited states are indicated in table 3 by grouping pairs of orbitals within parentheses. Single excitations to $4a_1$ and $4b_1$ are found at transition energies in excess of 30,000 cm^{-1}, as previously found for the mononuclear clusters. Again, these were not explored in depth.

Table 4
Transition energies (T) and electric-dipole oscillator strengths (f) for d–d transitions from the $^4A_2$ ground state of the **fac-Cr(III)** cluster.

Transition	T (cm^{-1})	$f \times 10^5$
$1\,^4A_1 \leftarrow 1\,^4A_2$	8,500	0[a]
$1\,^4E \leftarrow 1\,^4A_2$	11,300	43
$2\,^4E \leftarrow 1\,^4A_2$	16,200	37
$2\,^4A_2 \leftarrow 1\,^4A_2$	18,000	29
$3\,^4A_2 \leftarrow 1\,^4A_2$	19,800	25
$3\,^4E \leftarrow 1\,^4A_2$	32,800	42

[a] Symmetry forbidden in C_{3v}.

3.3. Mononuclear Cr(III) sites

Even though the emphasis of the present contribution lies on divalent chromium species, it was deemed necessary to include also Cr(III) species in order to identify transitions that may be used to distinguish the two oxidation states from one another. The ground state of the **fac-Cr(III)** cluster shown to the left in figure 2, is well described by the electron configuration $(1a_1)^1(1e)^2$, high-spin coupled to $^4A_2$. Three out of the five lowest excited states derive from the singly-excited $(1a_1)^1(1e)^1(2e)^1$ configuration, giving rise to states of A_1, E and A_2 symmetry in C_{3v}. Transitions to the $1\,^4A_1$ state, computed at 8,500 cm^{-1}, is electric-dipole forbidden. The first transition to receive appreciable intensity goes to $1\,^4E$, at 11,300 cm^{-1}. This state contains some mixing with the $(1e)^2(2e)^1$ configuration, which in turn is dominating the third excited state, $2\,^4E$, at 16,200 cm^{-1}. However, both $(1e)^1(2e)^2$ and $(1a_1)^1(1e)^1(2e)^1$ provide important contributions to $2\,^4E$.

The two next excited states, of $^4A_2$ symmetry, are mainly described by the $(1a_1)^1(1e)^1(2e)^1$ and $(1a_1)^1(2e)^2$ configurations. The mixture of these two configurations is important with respect to the strength of the associated dipole transitions, *i.e.*, the transition-dipole moment is expected to correlate with the weight of the singly-excited configuration. Since $2\,^4A_2$ and $3\,^4A_2$ have quite similar energy it is conceivable that one of these peaks may become significantly stronger than the other. The main point here is that we expect an electric-dipole active band in the region of 18,000–20,000 cm^{-1}, possibly with some structure.

The fourth excited state of ^4E symmetry lies some 33,000 cm^{-1} higher in energy than the ground state. It is mainly described by the $(1e)^1(2e)^2$ configuration, but borrows dipole intensity through interaction with singly-excited configurations. From the orbital energy diagram in figure 2, the first excitation to the second-lowest virtual orbital, $2a_1$, gives rise to a ^4E term. Using the energy of $4\,^4E$ as a lower limit, we can conclude that excitations to virtual orbitals with notable Cr 4s character lies above the d–d region in the spectrum, as was the case for Cr(II) sites.

4. Discussion

It is of interest to compare our computed d–d transition energies to those observed for the CO-reduced Phillips catalyst. Considering only electric-dipole-allowed transitions, the calculations give rise to bands at the following positions (cluster models): ∼5,000 cm^{-1} (**I, D**), ∼8,500 cm^{-1} (**T**), ∼10,000 cm^{-1} (**I, D**), ∼11,000 cm^{-1} **(fac-Cr(III))**, ∼12,500 cm^{-1} (**T**), ∼16,000 cm^{-1} (**fac-Cr(III)**), and ∼18,000–20,000 cm^{-1} (**fac-Cr(III)**).

Weckhuysen *et al.* conducted a literature survey of the DRS absorption bands of the CO-reduced Phillips catalyst [6], and it is evident that the reported spectral characteristics vary with both sample preparation and what is regarded to constitute a band. We will base our comparison on an extensive study conducted by Zecchina *et al.*, as well as later work by Weckhuysen and coworkers.

There are no experimental reports on band maxima as low in energy as 5,000 cm^{-1}; we can only conjecture that this may be due to lower-than-computed intensities or limitations during recording of the spectra. The first observed band is found at 7,500–8,000 cm^{-1} and assigned to coordinatively unsaturated Cr(II) [25,26,5], in agreement with our result for the **T** cluster. The next band was observed by Zecchina *et al.* at 10,000 cm^{-1} [10], as a shoulder to another band at ∼12,500 cm^{-1}. Weckhuysen *et al.* observe the same bands [6], and both groups see these transitions as evidence for more than one coordinative situation of Cr(II). It is suggested that the ∼12,500 cm^{-1} band may be ascribed to chromium in an octahedral coordination, while the band at 10,000 cm^{-1} may be due to a Cr^{2+} ion in a lower symmetry [6]. Our calculations lend support to the main conclusions from the experimental studies; the two bands in question may be assigned to divalent chromium species that are differing in the local geometry about the metal. However, we find the 10,000 cm^{-1} band to be indicative of chromium in a rather unstrained geometry, either bound as a mononuclear species to silica or as part of a dinuclear surface species. The band at higher energy would then correspond to a more strained mononuclear Cr(II) species, characterized by a narrow ∠OCrO angle.

Cr(III) species may also give rise to dipole-active transitions in this energy region, as evident from the transition computed at ∼11,000 cm^{-1} for the **fac-Cr(III)** cluster. Our cluster is probably too strained to be representative for Cr(III) species at the silica surface; one may easily envisage distortions to local C_s symmetry that will relieve the strain while keeping the pattern of three covalent ester linkages to the surface. This implies that while we expect the **fac-Cr(III)** cluster to constitute a useful model, individual transition energies may well be off by 1,000 cm^{-1} compared to what is correct for the majority of Cr(III)-species at the silica surface. Experimental spectra show no signs of a band at ∼11,000 cm^{-1}, suggesting that this band is indeed shifted into either of the 10,000 cm^{-1} and ∼12,500 cm^{-1} bands. Based on the higher intensity of the latter [10], we suggest this band to receive intensity from both Cr(III) and pseudo-tetrahedral Cr(II)-species.

Weckhuysen *et al.* [6] observe bands also at 15,500 and 19,500–21,000 cm^{-1} and assign these to Cr(III) species. This is in excellent agreement with our calculations, given that the energy of the second band is computed some 1,000 cm^{-1} too low. Again, this is well within reach by relaxation to a less symmetrical geometry than the one realized in our cluster. Zecchina *et al.* observe the ∼15,000 cm^{-1} transition only as a shoulder, yet make the same assignment to Cr(III) [10].

From the discussion thus far, there are some notable differences between the d–d spectra recorded by Zecchina *et al.* [10] for chromium on pyrogenic silica, and those reported by Weckhuysen *et al.* [3], using sol–gel silica as support. DRS spectra of reduced catalysts based on pyrogenic silica show two main peaks, at 8,000 and 12,500 cm^{-1}, respectively, corresponding to tetrahedral mononuclear Cr(II) sites. Additionally, a shoulder is reported [10] at 10,000 cm^{-1}, possibly due to a small population of dinuclear Cr(II) sites. Alternatively, it may be taken in evidence of a bimodal distribution of mononuclear Cr(II) sites with respect to the ∠OCrO angle.

In DRS spectra of reduced catalysts based on sol–gel silica [3], the first peak is found at 10,000 cm^{-1}, with no sign of a shoulder at the low-energy side. A likely explanation is the merger of the two first bands observed by Zecchina *et al.* [10], due to an increase in the Cr(II) dinuclear-to-mononuclear ratio. The position of the 12,500 cm^{-1} peak is not affected by the shifted position of the first peak, in agreement with this interpretation. Noteworthy, the band at 15,000 cm^{-1} is observed irrespective of the support type, indicating a small Cr(III) population in both cases.

The good correspondence between our calculated and the observed d–d transition energies support the widely accepted view of divalent chromium as the main surface species after reduction of the catalyst. However, assuming that silanol and siloxane moieties may coordinate weakly to Cr(II) sites without significantly changing the d–d transition energies, this does not exclude a population of chromium species that are coordinatively less unsaturated than our cluster models. The lack of reports of a ∼5,000 cm^{-1} band may indicate that weak coordination of additional ligands may affect intensities more than peak positions.

5. Conclusion

In this study, theoretical cluster models have been used to compute d–d transition energies and electric-dipole oscillator strengths for mononuclear and dinuclear Cr(II) species as well as mononuclear Cr(III) species. The computed transition energies agree well with what is observed experimentally, lending credibility to our results.

The d–d electronic spectrum contains several bands that may be used to identify specific coordination and oxidation states of chromium. In particular, the band at ∼8,500 cm^{-1}

is unique to mononuclear Cr(II) with a narrow ∠OCrO angle ("tetrahedral" site). Furthermore, transitions at ∼16,000 and ∼18,000–20,000 cm^{-1} are characteristic for Cr(III). A shoulder at ∼10,000 cm^{-1} is, on the other hand, found to receive contributions from both mono- and dinuclear Cr(II), and possibly also from Cr(III). For samples that are fully reduced to Cr(II), this band may be useful to identify chromium sites with a wide ∠OCrO angle. The same reasoning applies to the band at ∼12,500 cm^{-1}, in the absence of the Cr(III)-specific bands; this peak may serve to quantify tetrahedral Cr(II) sites. In the energy range below 30,000 cm^{-1}, we have not found any transitions well suited for quantification of dichromium species.

Acknowledgement

The Research Council of Norway is gratefully acknowledged by financial support as well as a grant of computer time (Programme for Supercomputing).

References

[1] B.M. Weckhuysen and R.A. Schoonheydt, Catal. Today 49 (1999) 441.
[2] B.M. Weckhuysen and R.A. Schoonheydt, Catal. Today 51 (1999) 215.
[3] B.M. Weckhuysen, I.E. Wachs and R.A. Schoonheydt, Chem. Rev. 96 (1996) 3327.
[4] M.P. McDaniel, Adv. Catal. 33 (1985) 47.
[5] B. Fubini, G. Ghiotti, L. Stradella, E. Garrone and C. Morterra, J. Catal. 66 (1980) 200.
[6] B.M. Weckhuysen, L.M. De Ridder and R.A. Schoonheydt, J. Phys. Chem. 97 (1993) 4756.
[7] G. Ghiotti, E. Garrone and A. Zecchina, J. Mol. Catal. 46 (1988) 61.
[8] B. Rebenstorf, J. Polym. Sci. A 29 (1991) 1949.
[9] B.M. Weckhuysen, R.A. Schoonheydt, J. Jehng, I.E. Wachs, J. Cho, R. Ryoo, S. Kijlstra and E. Poels, J. Chem. Soc. Faraday Trans. 91 (1995) 3245.
[10] A. Zecchina, E. Garrone, G. Ghiotti, C. Morterra and E. Borello, J. Phys. Chem. 79 (1975) 966.
[11] A.D. Becke, J. Chem. Phys. 98 (1993) 5648.
[12] S.H. Vosko, L. Wilk and M. Nusair, Can. J. Phys. 58 (1980) 1200.
[13] C. Lee, W. Yang and R.G. Parr, Phys. Rev. B 37 (1988) 785.
[14] M.J. Frisch *et al.*, Gaussian 98, Revision A.9 (1998).
[15] Ø. Espelid, K.J. Børve and V.R. Jensen, J. Phys. Chem. A 102 (1998) 10414.
[16] C.W.J. Bauschlicher, S.R. Langhoff and L.A. Barnes, J. Chem. Phys. 91 (1989) 2399.
[17] A. McLean and G. Chandler, J. Chem. Phys. 72 (1980) 5639.
[18] B.O. Roos, K. Andersson, M.P. Fülscher, P.-Å. Malmqvist, L. Serrano-Andrés, K. Pierloot and M. Merchán, Adv. Chem. Phys. 93 (1996) 216.
[19] K. Andersson *et al.*, MolCas 4.1 (1997).
[20] B.O. Roos, in: *Ab Initio Methods in Quantum Chemistry*, ed. K.P. Lawley (Wiley, New York, 1987).
[21] C.W.J. Bauschlicher and S.R. Langhoff, Chem. Rev. 91 (1991) 701.
[22] P.-Å. Malmqvist, in: *Molecules in the Stellar Environment. Lecture Notes in Physics*, Vol. 428, ed. U.G. Jørgensen (Springer, New York, 1994).
[23] Ø. Espelid and K.J. Børve, J. Catal. 195 (2000) 125.
[24] B. Civalleri, E. Garrone and P. Ugliengo, Chem. Phys. Lett. 294 (1998) 103.
[25] G. Ghiotti, E. Garrone, G.D. Gatta, B. Fubini and E. Giamello, J. Catal. 80 (1983) 249.
[26] H.-L. Krauss, B. Rebenstorf and U. Westphal, Z. Anorg. Allg. Chem. 414 (1975) 97.